Earth and Planetary Science Letters 369–370 (2013) 178–187

Contents lists available at SciVerse ScienceDirect

Earth and Planetary Science Letters

journal homepage: www.elsevier.com/locate/epsl

Thermal–petrological controls on the location of earthquakes within subducting plates

Geoffrey A. Abers [a,*], Junichi Nakajima [b], Peter E. van Keken [c], Saeko Kita [b], Bradley R. Hacker [d]

[a] Lamont-Doherty Earth Observatory, Columbia University, PO Box 1000, 61 Rte 9W, Palisades, NY 10964, USA
[b] Research Center for Prediction of Earthquakes and Volcanic Eruptions, Graduate School of Science, Tohoku University, Aramaki Aza-Aoba, Aoba-ku, Sendai 980-8578, Japan
[c] Department of Geological Sciences, University of Michigan, Ann Arbor, MI 48105, USA
[d] Department of Earth Science, University of California, Santa Barbara, CA 93109-9630, USA

ARTICLE INFO

Article history:
Received 14 August 2012
Received in revised form
26 January 2013
Accepted 18 March 2013
Editor: L. Stixrude
Available online 17 April 2013

Keywords:
subduction
intermediate-depth earthquakes
thermal models
metamorphic devolatilization

ABSTRACT

We find that in young and warm subducting plates, earthquakes occur just below the Moho. In older plates, earthquakes occur throughout the subducting oceanic crust, as well as the subducting mantle. We document this behavior in several subduction zones where there are independent constraints on earthquake locations and slab structure, specifically for northern and southern Japan, Alaska, and Cascadia. The differences in earthquake depth relative to subducting crust may reflect large differences in temperature and thus locations of major dehydration reactions. In colder slabs, the crust passes through blueschist-facies dehydration reactions, while in Cascadia and Nankai the major dehydration reactions in crust may be due to zoisite- and amphibole-breakdown or associated melting. The cold paths allow more mineral-bound H_2O to be retained within the crust at shallow depths, eventually released upon dehydration over shorter time intervals than warm paths. The cold path dehydration reactions also result in net positive volume changes of solid+fluid, with solid volume decreasing less than the volume of H_2O produced. On hot paths the net volume changes are negative, with solid volumes decreasing more than the volume of H_2O produced. The difference in behavior could drive a net increase in pore pressure upon dehydration for the cold but not the hot crustal paths. The difference in rate of release in H_2O, and difference in sign of net system volume change may promote seismogenesis in cold subduction zones but inhibit it in the crust of warm slabs. Within the mantle of the downgoing plate earthquakes mostly occur where serpentine is stable or breaks down, in both settings.

1. Introduction

While the largest earthquakes in subduction zones lie on interplate thrust faults, seismicity continues much deeper within the downgoing slab, well past the apparent downdip limit of stick-slip behavior on the thrust zone. These deeper earthquakes seem to occur at conditions at which "normal" frictional conditions do not operate, leading to decades of speculation about their origins (e.g., Wadati, 1928; Raleigh and Paterson, 1965; Frohlich, 1989; Green and Houston, 1995; Kirby et al., 1996; Jung et al., 2004). As they descend subducting plates undergo a series of dehydration reactions, releasing fluids and increasing density of the remaining solid (e.g., Schmidt and Poli, 1998; van Keken et al., 2011) over depth ranges similar to those where many earthquakes occur. This has led many to argue that the dehydration process somehow facilitates earthquakes (Hacker et al., 2003b). Other possibilities, such as thermally modulated ductile instabilities in certain sets of conditions have also been proposed (Ogawa, 1987; Kelemen and Hirth, 2007). Differentiating between them may rely upon a better understanding of the physical conditions and systematics of these earthquakes in situ.

As imaging and hypocentral determination have become more accurate, it is becoming possible to tell where earthquakes lie relative to subducting crust at depths less than 200–300 km (e.g., Abers et al., 2006; Kita et al., 2006). Several recent advances in imaging methods and instrumentation have greatly increased the precision of both hypocenters and determination of the internal structure of slabs, such as through high-resolution tomography and migration of receiver functions. These advances are particularly successful in regions that have seen the deployment of dense temporary arrays of broadband seismographs or are characterized by high-quality dense long-term monitoring (e.g., in Japan and North America) (Fig. 1). With a small number of such studies now available, it is now possible to evaluate systematics of subduction zone behavior at the scale of subducting crust.

* Corresponding author. Tel.: +1 845 365 8539; fax: +1 845 365 8510.
E-mail addresses: abers@ldeo.columbia.edu (G.A. Abers), nakajima@aob.gp.tohoku.ac.jp (J. Nakajima), keken@umich.edu (P.E. van Keken), kita@aob.gp.tohoku.ac.jp (S. Kita), hacker@geol.ucsb.edu (B.R. Hacker).

0012-821X/$ - see front matter © 2013 Elsevier B.V. All rights reserved.
http://dx.doi.org/10.1016/j.epsl.2013.03.022

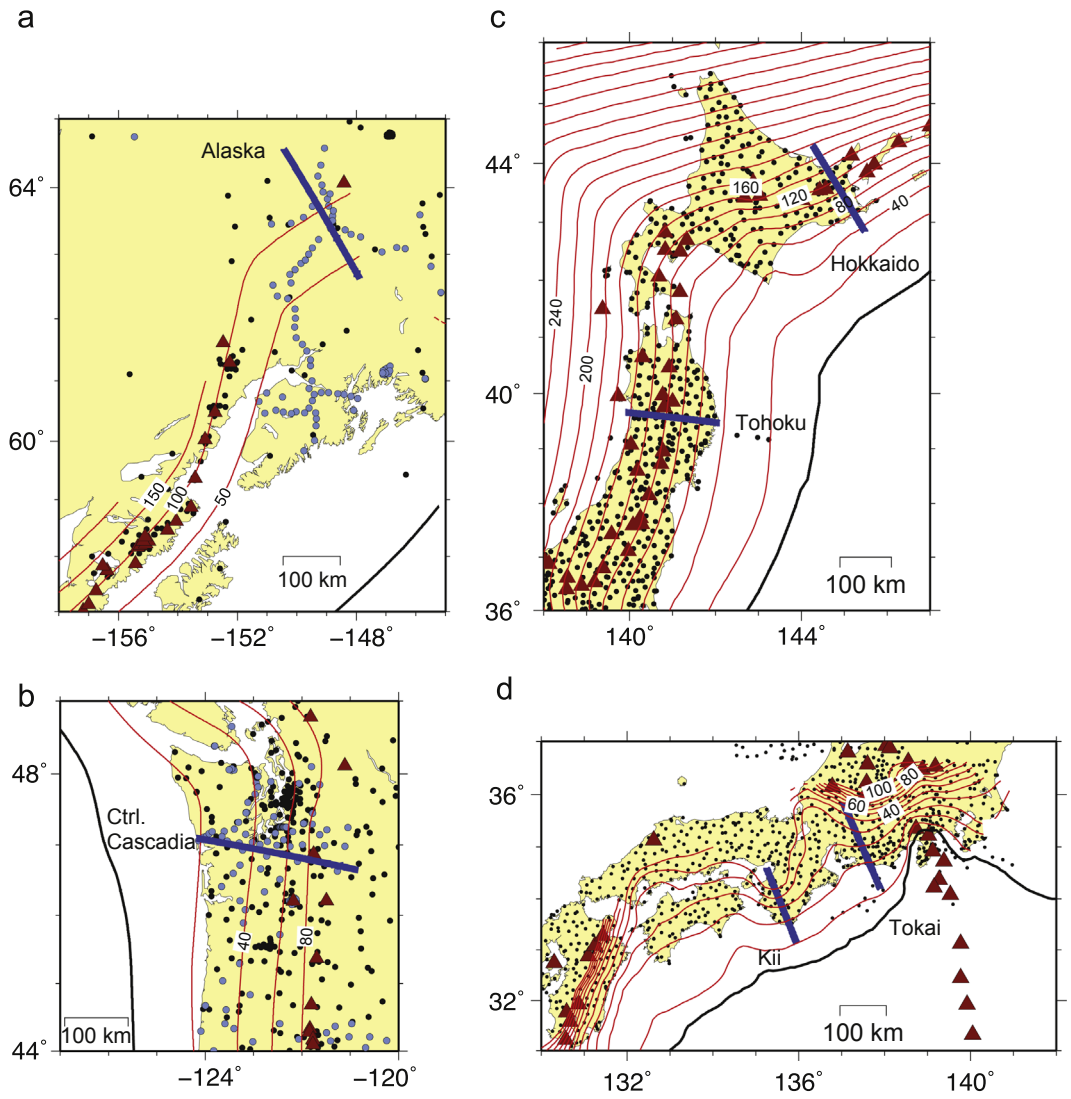

Fig. 1. Maps of study areas, showing location of cross sections analyzed (blue bars), trench (black line), contours to Wadati–Benioff Zone (red lines, depths in km labeled), and active volcanoes (red triangles). Black dots show permanent seismic stations, blue dots show temporary arrays used in this study. Volcanoes from Syracuse and Abers (2006) and updates. (a) Alaska, image transect following Abers et al. (2006); (b) Washington Cascades, image transect following Abers et al. (2009); (c) North Japan, transects following Kita et al. (2006, 2010b) with slab surface from Zhao et al. (1997) and Kita et al. (2010b); and (d) Southern Japan/Nankai Trough, transects following Hirose et al. (2008). (For interpretation of the references to color in this figure legend, the reader is referred to the web version of this article.)

The importance of high-resolution imaging is that it provides information on the location of both the plate interface and internal interfaces—particularly the Moho of the subducting oceanic plate—independent of the subduction geometry inferred from seismicity. These images now allow us to answer in a systematic way the question "Do earthquakes occur within subducting crust or mantle?" We find that the answer depends on the thermal state of the slab; for many slabs the upper-plane seismicity takes place within the subducting crust, but for the hottest slabs all seismicity lies just below the Moho. (In northern Japan a double seismic zone is observed, but in this study examines just the upper plane of intraslab earthquakes where differences between behavior of subducted crust and mantle can be most easily compared.)

In most subduction zones earthquakes can occur within subducting mantle, and mantle dehydration reaction boundaries are largely isothermal, so it is difficult to tell fluid release or thermal weakening are more important in these earthquakes. However, within the subducting crust we observe that earthquakes occur in cold slabs but not in warm ones, even though crust passes through the same temperature range in both. Hence, the behavior of earthquakes within the crust constrains the mechanisms by which earthquakes can be generated. The sign of volume change during metamorphic dehydration appears to drive this behavior; hot crust dehydrates through different mineral systems than cold crust, resulting in reactions that inhibit rather than promote excess fluid pressure. Thus, dehydration processes seem to play an important role in generating intermediate-depth earthquakes.

2. Observations of seismicity in well-characterized subduction zones

2.1. Alaska

The Pacific plate subducts beneath Alaska at 55 mm/yr (DeMets et al., 1994) within 15° of normal to the strike of the imaged slab. The age of the lithosphere at the trench is roughly 38 Ma (Atwater, 1989). In the easternmost section of the Aleutian trench normal Pacific oceanic crust does not subduct, but instead the 50–55 Ma Yakutat terrane has entered the trench and is subducting to a depth of at least 130 km (e.g., Bruns, 1983; Fuis et al., 2008; Ferris et al., 2003). Seismic velocities of the Yakutat terrane indicate that it consists of

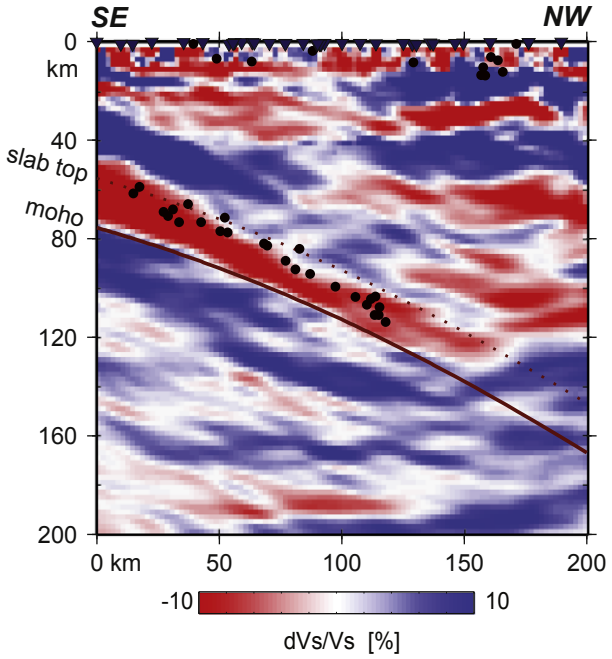

Fig. 2. Central Alaska subduction zone and seismicity, along the profile shown in Fig. 1a. Colored image shows migrated teleseismic P coda as dV_S/V_S (Rondenay et al., 2008, 2010); red corresponds to slow velocities and blue to fast. Data are sensitive to sharp gradients, which produce P-to-S scattering. Black circles show seismicity from the same array ("BEAAR", Broadband Experiment Across the Alaska Range), relocated in the same velocity model used as migration, along the same corridor. Solid and dotted line shows smooth polynomial fit to top and bottom of subducted crust, used in thermal modeling (Abers et al., 2006). (For interpretation of the references to color in this figure legend, the reader is referred to the web version of this article.)

anomalously thick gabbroic crust, similar to that of oceanic plateaus, varying from 30 to 15 km in thickness from east to west (Christeson et al., 2010; Worthington et al., 2012). The subducting plate has a dip of 5°, from the trench to 50 km depth, steepening to 25° dip at greater depth. This geometry, velocity and inferred plate age result in a thermal history that is comparable to many "cold" subduction zones around the world (Syracuse et al., 2010).

The Broadband Experiment Across the Alaska Range (BEAAR) seismic deployment (1999–2001) provided the first direct image of the subducting plate at 50–130 km depth (Ferris et al., 2003; Rossi et al., 2006; Rondenay et al., 2008, 2010). The same array, augmented by permanent seismic stations, constrains intermediate-depth seismicity with much greater precision than permanent networks (Abers et al., 2006). The fortuitous presence of thick crust makes it possible to map spatial variations in the location of seismicity with respect to the subducting crust. Seismicity is near the top of the subducting crust at depths <80 km and gradually descends to the subducting Moho as the plate deepens (Fig. 2). Both the seismicity and the imaged subducted crust terminate near 120–130 km depth, an observation used to infer that both are limited by the eclogitization of the subducted crust (Ferris et al., 2003; Rondenay et al., 2008), an inference supported by travel-time tomography (Eberhart-Phillips et al., 2006). All of these earthquakes lie inside the subducting crust, along a plane dipping roughly 2° more steeply than the plate interface (Abers et al., 2006).

Uncertainties in both hypocenters and slab surface depth depend largely on uncertainties in seismic velocity structure above the source, so they are correlated. Hypocentral errors are heavily dominated by velocity uncertainties rather than random picking errors. The same is true of depths to interfaces illuminated by mode conversions as with receiver functions. Both the subducting Moho and hypocenters are located by the BEAAR array by numerous and similar upgoing raypaths, sensitive to both P and S structures and in particular to the differential travel time between P and S waves. The relative and absolute uncertainties of these two data have been analyzed in some detail previously through the Monte Carlo simulations (Abers et al., 2006). Although random errors in both are 5–10 km from the BEAAR data, relative error is much less, so that all hypocenters lie within subducted crust or within 2–3 km of it for extreme cases.

2.2. Cascadia

Cascadia is a classic "warm" subduction zone, forming the hot thermal endmember of slab surface conditions (Oleskevich et al., 1999). At the trench, the subducting Juan de Fuca plate has an age of 6–9 Ma and subducts obliquely at rates of 35–45 mm/yr. The resulting downdip subduction rate is 25–35 mm/yr beneath Oregon and Washington. The slow subduction of young oceanic lithosphere make this one of the hottest slabs globally (Wada and Wang, 2009; Syracuse et al., 2010) and is predicted to undergo dehydration of the sedimentary and igneous crust well before reaching sub-arc depths (Hacker, 2008; van Keken et al., 2011). Intraplate seismicity is rare, largely confined to the region north of 47°N or near the Mendocino triple junction (e.g., Wada et al., 2010).

Three dense broadband seismometer transects have been deployed across the Cascadia forearc and arc in central Oregon (Li and Nabelek, 1999; Rondenay et al., 2001), Vancouver Island (Nicholson et al., 2005), and central Washington (Abers et al., 2009). All show a similar structure of the slab with a low-velocity channel resembling subducting oceanic crust that dips landward from the coast to depths of 40–50 km. The Moho appears to continue as a weak velocity contrast to greater depths (Fig. 3). The Washington section samples the most seismogenic part of the Juan de Fuca plate. Most of the large ($M>6.5$) intraslab earthquakes in Cascadia occur along that section (Ichinose et al., 2004) and the deepest earthquakes in Cascadia lie under Mt. Rainier (47°N) at approximately 90 km depth. Otherwise, the seismicity is relatively feeble compared with the other subduction zones and terminates at shallow depths, consistent with high slab temperatures (Hacker et al., 2003b).

Careful relocation of hypocenters with the same dense array used for imaging shows that virtually all intraslab earthquakes lie at or just below the Moho (Abers et al., 2009). The seismicity is separated from episodic tremor, which lies along the plate interface (Brown et al., 2009). It is not obvious that any seismicity lies within subducted crust. A slightly different interpretation has been made from comparing wide-angle reflections beneath the Olympic

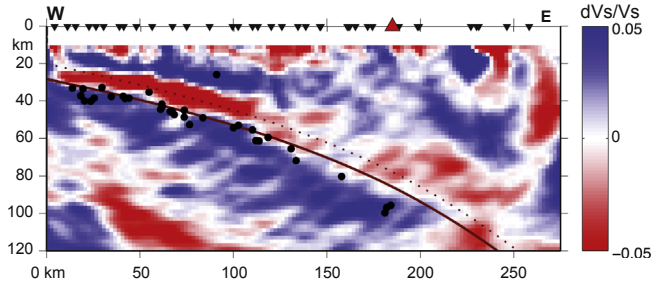

Fig. 3. Central Cascadia subduction zone and seismicity, along profile shown in Fig. 1b. Colored image shows migrated teleseismic P coda as dV_S/V_S (Abers et al., 2009), as in Fig. 2. Black circles show seismicity located by the same array ("CAFE", Cascadia Arrays For EarthScope), relocated in the same velocity model used as migration, along the same corridor. Solid and dotted line shows smooth polynomial fit to top and bottom of subducted crust, used in thermal modeling (van Keken et al., 2011). Red triangle: Mt. Rainier volcano; inverted black triangles: seismic stations used. (For interpretation of the references to color in this figure legend, the reader is referred to the web version of this article.)

peninsula with seismicity by Preston et al. (2003), who argued that a few of the deepest earthquakes may lie within the lowermost subducting crust. However, most of the inferred crustal earthquakes are downdip of where the reflector is well established in that study, and it is possible that they are in the mantle section instead.

As with Alaska, the hypocenters and slab surface image derive from similar stations and ray paths, so the relative location of hypocenter and slab surface is small. Since the slab surface here is only 30–80 km deep, ray paths are typically half as long as in Alaska, and errors due to velocity uncertainty are proportionately less. Velocities from P-wave active-source imaging and ambient-noise S-wave tomography have path-averaged uncertainties above the slab of typically 0.1 km/s and never more than 0.2 km/s (Calkins et al., 2011). Monte Carlo simulations in which the velocities are perturbed and both slab depth (from receiver functions) and hypocenters (from travel times) are redetermined show that the absolute location of hypocenters or slab surface may vary by 3–4 km, but the relative variation is less than 2 km. In all simulations, earthquakes lay below the Moho or at most 1–2 km above it, with one exception, at $x=55$ km in Fig. 3. Finally, active-source reflections nearby (Parsons et al., 1998) show an oceanic crust at the coastline that is within 1–2 km in depth from that shown in Fig. 3, so the earthquake imaging shows Moho depth that is correct in an absolute sense.

2.3. Northern Japan

The 120–130 Ma Pacific plate subducts beneath Northern Japan with a convergence velocity roughly 80 mm/yr, making it an archetypical "cool" subduction zone (Peacock and Wang, 1999). Roughly 7 km thickness of oceanic crust is subducted here, 6 km of basement (Takahashi et al., 2004) plus some sediment. The main Wadati–Benioff zone dips approximately 30° beneath the island of Honshu, with seismicity extending at that dip to nearly 700 km. Thermal models here predict gradual dehydration of oceanic crust at sub-arc depths (Syracuse et al., 2010; van Keken et al., 2011), consistent with sharp velocity contrasts between subducting crust and mantle extending to at least 100 km in receiver functions (Kawakatsu and Watada, 2007) and high-frequency mode conversions (Matsuzawa et al., 1986). These mode conversions have been well studied, and provide precise constraints on slab geometry that are independent of seismicity (Zhao et al., 1997; Kita et al., 2010a).

Clearly some of the seismicity here takes place in the mantle (Nakajima et al., 2009a; Kita et al., 2010a), as evident from the 30–40 km thick double seismic zone. However, most of the upper-plane seismicity seems confined to the subducting crust (Igarashi et al., 2001; Kita et al., 2010a). The crust has been well defined by mode-converted waves and tomography (Tsuji et al., 2008; Nakajima et al., 2009b) and the predicted eclogite-generating dehydration phase transformations (Hacker et al., 2003a, 2003b) roughly correlate with pulses of seismicity in the upper-plane seismic belt (Kita et al., 2006; van Keken et al., 2012) (Fig. 4). Because of the low temperatures of this plate, crust passes through dehydration reactions over a wide depth range, perhaps explaining the abundance of seismicity within the crust here. At Eastern Hokkaido the subduction rate, plate age, and the locations of WBZ seismicity all appear similar, although the corner between the two subduction zones may be colder (Tanaka et al., 2004; Kita et al., 2010b).

The slab surface beneath Tohoku is estimated by travel-time differences between the mode-converted and direct phases (PS-P/SP-S), and errors in the relative location between the slab surface and hypocenters are 1–2 km (Zhao et al., 1997). Errors in hypocenters are estimated to be ~1 km (Kita et al., 2010b), but the upper limit of seismicity is consistent well with the slab interface estimated by Zhao et al. (1997). Slab surface and Moho boundaries independently determined from receiver functions (Kawakatsu and Watada, 2007) lie within 1–2 km of these, to depths of 100 km. Therefore, uncertainties in the relative position between the upper-plane seismicity and the surface are at most 2–3 km and these errors do not affect our conclusion that much of the upper plane seismicity occurs in the oceanic crust. In Hokkaido, at depths less than 80 km the slab surface is constrained to pass through thrust zone earthquakes and repeating earthquakes known to lie on it (Kita et al., 2010a); uncertainties at those depths are similar to Tohoku. Deeper the Hokkaido slab surface is extrapolated smoothly and inferred from seismicity, so less accurate, but applying the same procedure to Tohoku gave a nearly identical geometry within 1–2 km as from using mode conversions (Kita et al., 2010a, 2010b). Most Hokkaido results here come from earthquakes >80 km deep where clearly most earthquakes lie within subducted crust.

2.4. Nankai trough: Tokai, Kii

The young (~20 Ma) Philippine Sea plate subducts beneath southern Japan at the Nankai trough. While plate motion constraints are somewhat more ambiguous and there is considerable upper-plate deformation, best estimates suggest oblique subduction at 30–60 mm/a (Seno et al., 1993; Miyazaki and Heki, 2001; Loveless and Meade, 2010), averaging 40–45 mm/a. Off the central parts of the Nankai trough, the 15–26 Ma Shikoku back-arc basin subducts presently (Okino et al., 1994). The resulting relatively

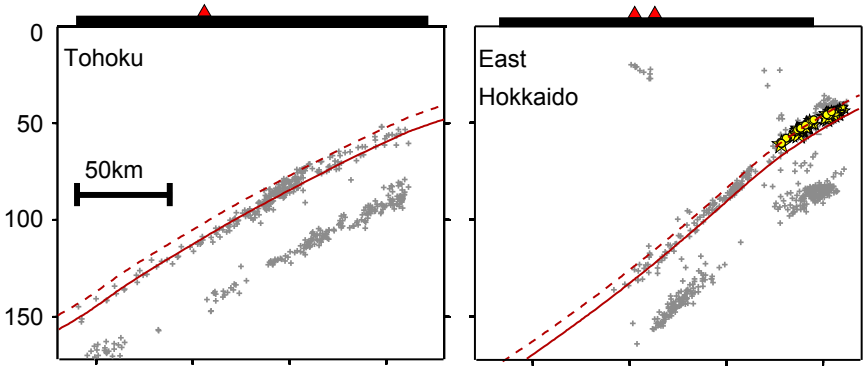

Fig. 4. Northeastern Japan subduction zone and seismicity (similar to Fig. 2 of Kita et al., 2010b), along the profile shown in Fig. 1c. Gray dots show earthquakes that occur within 10 km from each profile. Solid red lines show the estimated plate interface (Zhao et al., 1997; Kita et al., 2010b), and dashed red line shows estimated Moho at 7 km below the top of the Pacific plate. Yellow stars and yellow circles respectively show epicenters of small repeating earthquakes (Uchida et al., 2009) and low-angle thrust-type events (Kita et al., 2010a). Horizontal thick black lines show the area of the land. (For interpretation of the references to color in this figure legend, the reader is referred to the web version of this article.)

young and slow converging plate is a warm end-member (Peacock and Wang, 1999), consistent with the lack of WBZ seismicity deeper than about 60 km. Unlike Cascadia or indeed most other subducting plates, the geometry within the thrust zone is highly contorted with strong variations in dip along strike (Fig. 1d).

The Nankai subduction zone also exhibits abundant slow slip events (Obara, 2002) that show thrust-faulting mechanisms (Ide et al., 2007; Ito et al., 2007) and define the plate contact zone at depth (Kato et al. 2010). By contrast, regular earthquakes lie within the downgoing plate and are several km deeper than the thrust zone defined by low frequency earthquakes. Most appear to lie within the subducting mantle (Shelly et al., 2006; Hirose et al., 2008; Kato et al., 2010) (Fig. 5). There may be some variation along strike in the relative location of Moho to intraslab seismicity, but the careful mapping of the thrust zone by low-frequency earthquakes shows in all cases a gap between the plate boundary and regular intraslab earthquakes that is roughly the thickness of the subducted crust. Thus Nankai, like Cascadia, has earthquakes principally within the mantle rather than within the crust of the subducting plate.

For Nankai, the upper surface of the Philippine Sea slab is delineated based on the locations of non-volcanic tremors and the low-velocity oceanic crust, and it agrees well with the slab surface determined by seismic refraction surveys (Hirose et al., 2008). Hirose et al. (2008) checked the effect of differences in seismic velocity models on hypocenter locations and confirmed that the shifts of hypocenters are small ($\sim$2 km). In addition, receiver function analyses, which can constrain the oceanic Moho independent of seismicity, have determined the oceanic Moho immediately above the seismicity (e.g., Yamauchi et al., 2003; Kato et al., 2010), supporting the absence of seismicity in the oceanic crust.

2.5. Other examples

One useful metric to compare the thermal state of these regions is the "thermal parameter" (Molnar et al. 1979; Kirby et al., 1996), $\Phi = AV \sin\delta$, where A is the incoming plate age, V is the arc-normal convergence velocity, and δ its dip. This product scales to several aspects of the thermal structure, such as the maximum depth of isotherms within the deep slab, and predicts well the plate-interface temperature along the thrust zone in more complicated models (Syracuse et al., 2010). We will use the values from Syracuse et al. (2010) unless otherwise indicated. For Cascadia and Nankai, Φ is 100–130 km and 450 km respectively, whereas for Alaska it is roughly 2750 km (re-estimated for adjacent Pacific lithosphere, from updated geometry) and 5000–5700 km for Tohoku and eastern Hokkaido. Thus, a large difference in thermal state separates these two populations.

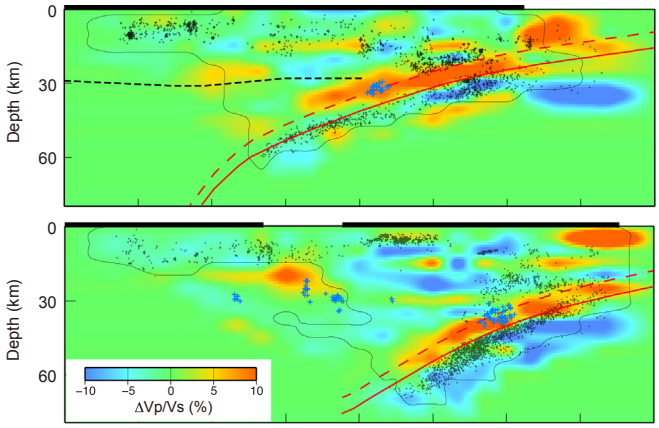

Fig. 5. Cross sections through the Southeast Japan/Nankai subduction zone, at (top) Tokai and (bottom) Kii peninsula; locations in Fig. 1. Images show shear wave velocity variations and relocated hypocenters from Hirose et al. (2008); black dots show regular earthquakes, while blue crosses show deep low frequency earthquakes, projected from 15 km of line. Black bars at top denote land area; red dashed and solid lines show inferred slab surface and Moho of subducting plate, respectively, from Hirose et al. (2008). (For interpretation of the references to color in this figure legend, the reader is referred to the web version of this article.)

Costa Rica shows seismicity apparently within subducted crust, beneath the Nicoya Peninsula (Φ is 970–1100 km, re-estimated here from where locations are well determined; DeShon et al., 2006); Receiver functions here show a complicated Moho (MacKenzie et al., 2010). Beneath northern New Zealand active-source imaging shows the thickened Hikurangi plateau subducting at shallow depths. Its crust is seismogenic (e.g., Bassett et al., 2010) and Φ is 2420 km. A few well-studied sections of the Nazca plate subducting beneath the Andes ($\Phi\sim$1070–1780 km) seem to show seismicity above the Moho of the subducted crust at least at depths <100 km in receiver functions (Yuan et al., 2000; Sodoudi et al., 2011).

3. Constraints on subduction zone seismogenesis

3.1. Summary and comparison of observations

In most subduction zones the subducting oceanic crust, whether normal or plateau, is seismogenic to or past sub-arc depths. The obvious exceptions are the few very warm subducting plates with $\Phi < 500$ km (e.g. Nankai and Cascadia), where the subducting crust is largely aseismic. The Cocos plate at Central America (Φ=970–1100) and the Nazca plate at north-central Chile (Φ=1070–1780) behave as "cold" subduction zones in that the oceanic crust is seismogenic. Hence, it appears that the critical behavior changes at approximately Φ=500–1000 km. Crust that is too hot subducts aseismically, whereas the underlying mantle lithosphere can generate earthquakes. This behavior becomes clear in comparing histograms of earthquake distribution for the six well-characterized transects discussed above (Fig. 6). Although a few earthquakes may occur in the crust of the Tokai section, in general the three "hot slab" segments show most or all of their seismicity is in the mantle of the subducting plate (or in the crust of the overriding plate, at shallow depths). By contrast, the cooler subduction-zone segments (Alaska, Hokkaido and Tohoku) all show a peak in earthquake distribution within the subducting crust, with variable amounts of seismicity within the underlying mantle. These observations suggest a control on Wadati–Benioff Zone seismicity that involves both temperature and p–T path.

3.2. Thermal models

In order to more quantitatively assess the conditions at which earthquakes occur, we calculate for each subduction zone segment a two-dimensional thermal model to predict slab temperatures. Unless otherwise noted, all models are constructed in the same manner as in Syracuse et al. (2010). The slab surface is defined as the top of the sediments, as constrained by mode conversions and thrust-zone earthquakes, and parameterized by a natural spline through six or seven points. At shallow depths the plate motion is localized to this boundary, while viscous wedge flow couples beyond 80 km depth. The wedge rheology is that of a composite diffusion and dislocation creep law for dry olivine. No shear heating is imposed. Unless otherwise noted the mantle potential temperature is set at 1421.5 °C following the GDH1 plate model (Stein and Stein, 1992). We also use the GDH1 plate model for the temperature structure of the incoming lithosphere.

The models all have a slab geometry described by the interpolation with the slab surface, shown as dashed red lines in

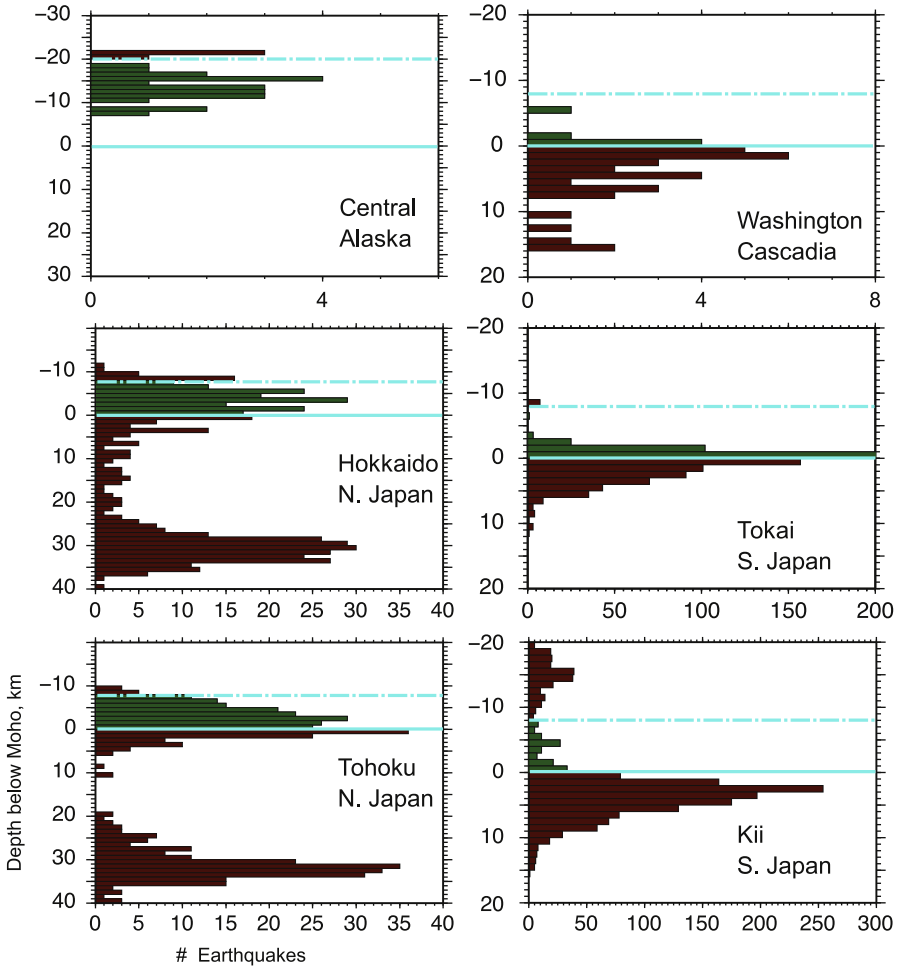

Fig. 6. Numbers of earthquakes vs. depth below Moho of subducting plate, measured vertically. Seismicity is from focused experiments for Alaska and Cascadia after relocation and selection of high-quality hypocenters (Figs. 2 and 3) or from inversions of long-term monitoring data (Japanese subduction zones; Figs. 4 and 5). Green bars correspond to subducting oceanic crust. Blue solid and dashed line represents subducting Moho and plate interface, respectively. Positive depth indicates seismicity within subducting mantle lithosphere. For Tokai, earthquakes 0–2 km above slab Moho are at deep end of the seismicity, where slab Moho is weakly defined. (For interpretation of the references to color in this figure legend, the reader is referred to the web version of this article.)

Figs. 2–5. For Alaska, the model is similar to that from Abers et al. (2006) but with an updated geometry following recent imaging (Kim et al., 2012). The age at the trench is set to the approximate age of the Yakutat terrane, 52.2 Ma. A mantle potential temperature of 1350 °C and a slightly faster-than-observed subduction velocity (65 mm/yr vs. 60 mm/yr) is presented as it shows a greater consistency between predicted blueschist-out boundary and the dipping plane of seismicity. We assume 2 km of sediment at the trench (Clift and Vannucchi, 2004). For the central Cascadia section, we assume an incoming plate age of 7.5 Ma. The convergence speed is 35 mm/y, with 2.2 km sediments at trench and 0.46 km of sediments subducting deeper than 15 km (see Syracuse et al., 2010).

The modeling for the two Nankai profiles (Tokai and Kii) is more complex. Previously (Syracuse et al., 2010) we assumed a 15 Ma old slab subducting at ~30 mm/yr. These parameters lead to a relatively cool slab with extensive blueschist at 40–50 km depth. There are several suggestions that the slab has a hotter temperature, however. At the trench, the age of the incoming plate varies from ~17 to 25 Ma depending on distance to the Shikoku ridge (where spreading stopped around 17 Ma; Okino et al., 1994). At the time of first subduction of the Shikoku ridge, then, the initial plate age should have been around 2–8 Ma. Kimura et al. (2005) argued that Nankai subduction was much slower at ~9 mm/yr before 4 Ma so slab that subducted before that date should be hotter than predicted by steady-state models. To approximate this time history, the models presented here have an incoming plate age that increases from 2 Ma to 19 Ma and the subduction speed is kept constant at 20 mm/yr. We assume that 1.5 km thick sediments enter at the trench and that 0.3 km of sediments subduct to depths > 15 km.

In northern Japan, we follow the modeling of van Keken et al. (2012) and use profiles based on the slab geometry determined by Zhao et al. (1997) and Kita et al. (2010a) (Fig. 4). For Tohoku this profile is identical to that of Kita et al. (2006), whereas for East Hokkaido we used the profile (b) from Kita et al. (2010b). The assumed age of the slab is 130 Ma. Due to the change in obliquity of the convergence of the Pacific plate and the trench the speed of subduction varies along the profile increases from 64.9 mm/yr (East Hokkaido) to 81.6 mm/yr (Tohoku). Bengtson and van Keken (2012) show that the use of the trench-normal cross-section with only trench-normal convergence velocity leads to a better approximation of the 3D temperature distribution compared to the alternative choice of a profile parallel to convergence direction.

For each model, we track the temperature at the slab surface and at the Moho (7 km deeper into the slab, except in Alaska where the Yakutat terrane subducts, and 20 km is used). We predict metamorphic facies and mineral-bound H_2O content throughout the subducting plate following Hacker (2008) and van Keken et al. (2011). The calculations give quantitative estimates of the rates of

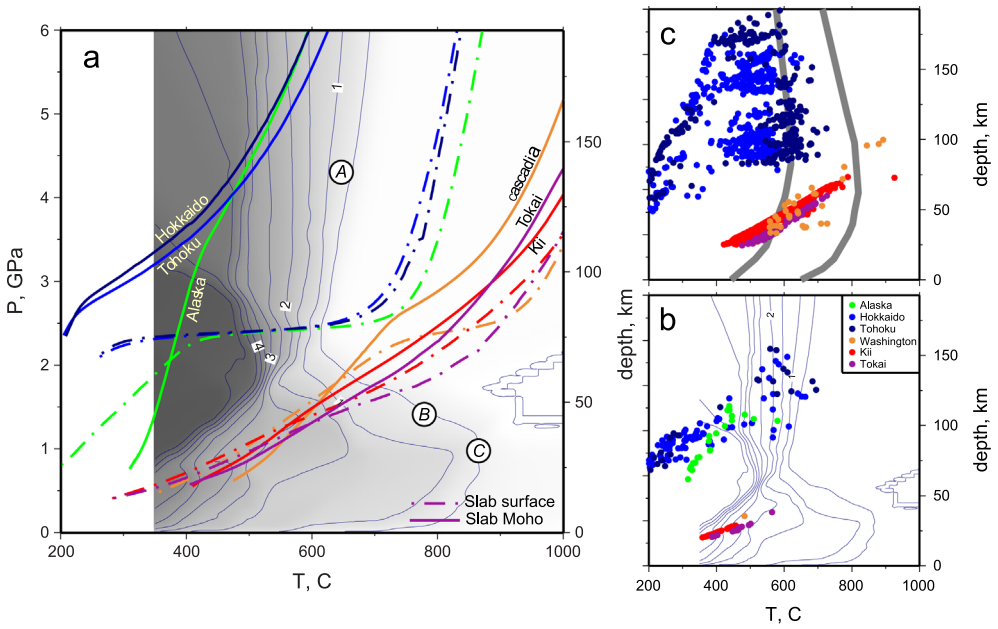

Fig. 7. (a) Predicted pressure–temperature paths for subducted crust, and expected dehydration. p–T paths are colored as labeled, solid for subducted Moho and dot-dashed for slab surface, calculated as described in text. Shading shows maximum H_2O contents in wt%, as labeled, for a hydrated metabasalt of MORB bulk composition (Hacker, 2008); major dehydration reactions indicated by circled numbers as "A" lawsonite breakdown, "B" zoisite breakdown, and "C" amphibole breakdown. Paths are drawn only at depths where earthquakes can be located from the six arrays discussed in text, so they do not extend updip out of seismic arrays. Note that the paths for hot and cold subduction zones intersect different dehydration reactions, largely blueschist dehydration for cold subduction zones and zoesite-amphibole breakdown for hot paths. (b) Depths and temperatures of earthquakes within crust, as defined in Fig. 6, from thermal models in (a). Thin lines are contours of H_2O content within hydrated metabasalt, from (a). (c) Depths and temperatures of earthquakes in subducting mantle. Gray lines show predicted breakdown of antigorite at ca. 600 °C and chlorite at 700–800 °C (Hacker et al., 2003a).

water production via dehydration. The resulting p–T paths show that the hot and cold slabs experience markedly different conditions (Fig. 7a). Cold slabs dehydrate at pressures >2 GPa (depths >80 km) and show 300–400 °C temperature changes between slab surface and Moho. By contrast, warm slabs all dehydrate at lower pressures, before reaching the hot flowing wedge at 80 km depth and show little variation in temperature between top and bottom of the subducted crust.

3.3. Earthquakes and p–T paths

It has been long argued that dehydration reactions can induce seismicity (e.g., Raleigh and Paterson, 1965; Hacker et al., 2003b). Because most earthquakes produce double-couple focal mechanisms at intermediate depths (Frohlich, 1989) the volume changes are unlikely to directly produce earthquakes and earthquake triggering is ascribed to secondary effects. These could include differential volume changes between metamorphosing basaltic crust and adjacent mantle (Kirby et al., 1996), the release of water and related pore-pressure changes (e.g., Wong et al., 1997; Dobson et al., 2002), or a more-complicated effect of the release, segregation and transport of water (e.g., Jung et al., 2004).

Our results place several constraints on the processes that allow earthquakes to occur (Fig. 7b and c). No earthquakes are seen at conditions where temperature $T>700$ °C (except for a handful of earthquakes at 60–90 km in Cascadia), consistent with the long-held understanding that earthquakes cannot occur where the earth is warm and weak (e.g., McKenzie, 1969). However, temperature alone cannot regulate seismogenesis. There are clearly temperatures where earthquakes occur in the mantle but not in the crust, so lithology matters. Also, even within the crust, seismogenesis seems to vary with the pressure–temperature (p–T) trajectory. Cold subduction zones show earthquakes within the crust to pressures of 4–5 GPa (125–160 km depth), some at temperatures of 500–650 °C. Crust in warm subduction zones passes through these same temperatures, albeit at lower pressures of 0.8–1.5 GPa, yet few earthquakes occur in crust there. We note that earthquakes may occur in oceanic crust at very shallow depth (<25 km or 0.8 GPa), but their locations are imprecise due to their offshore location.

3.4. Dehydration and fluid release

To evaluate these different thermal histories, we compare the calculated p–T trajectories to dehydration reactions predicted for a hydrated MORB composition. These calculations follow those of Hacker (2008) and are based on Gibbs free energy minimization (Connolly and Petrini, 2002), assuming a maximum of 5 wt% H_2O. We show results only at temperatures above 350 °C to avoid complications with poorly constrained activity models and disequilibrium. At high pressures the chief dehydration reaction is the (A) breakdown of lawsonite at 550–700 °C to garnet+clinopyroxene +white mica+H_2O (capital letters refer to Fig. 7). Dehydration is divariant with significant H_2O loss at lower temperatures. Isopleths of evolved H_2O are subparallel to the final breakdown reaction, which has a positive Clapeyron slope of 57 MPa/K at 3 GPa. The Hokkaido, Tohoku and Alaska crust should dehydrate in this region. At the same temperature, but lower pressure the dehydration of zoisite (B) comes into play. At lower pressure and higher temperature the phase relations are complicated by melting (e.g., Vielzeuf and Schmidt, 2001). Under the assumption that H_2O-saturated melting does not play a role the relevant reactions are (B) zoisite-dehydration and (C) amphibole-dehydration or melting. The former has not been extensively studied in mafic rocks (Lambert and Wyllie, 1972), but probably has a maximum temperature of 750 °C (Vielzeuf and Schmidt, 2001); the latter has been studied extensively (see summary in Moyen, 2011). The Nankai and Cascadia subduction zones cross these reaction boundaries.

The cold paths in northern Japan and Alaska subduct through blueschist-facies conditions, where lawsonite breakdown can

release up to 5 wt% H_2O. Much of this may be released fairly quickly, where the slab surface heats by 400 °C as it enters the hot flowing part of the mantle wedge near 80 km depth. This locally large release of water should significantly alter the surrounding region. Estimates of hydration of 0.8 wt% H_2O in the lower oceanic crust (Jarrard, 2003) probably preclude water saturation of the gabbros until temperatures exceed 600 °C, so their contribution is less than illustrated by the fully saturated case. By contrast, the hot-slab crust of Nankai and Cascadia cannot retain more than 2–3 wt% H_2O anywhere in the subducting crust at pressures >0.5 GPa, because it has not had long to cool since formation.

3.5. Fluid production rates

Along hot-slab paths, H_2O is released relatively gradually as the plate descends relative to cold-slab paths. These differences in the rate of H_2O production are enhanced by differences in subduction velocity, since the cold subduction zones subduct at two to three times the rate of hot ones. We illustrate this by calculating the fluid production rate and amount of free water predicted for subducting basalt crust (Fig. 8). Devolatilization is calculated along p–T paths following the top of the subducting crust, for a closed MORB–H_2O system in which H_2O cannot escape, again using a Gibbs free energy minimization method (Connolly and Petrini, 2002). For each mole of starting material we track the total mass of H_2O freed from the solid, the incremental volume of H_2O freed per reaction step, and the volume reduction of the remaining solid over reaction step. We repeated the calculation for a system in which free H_2O was removed at each calculation step (not shown), with very similar results but greater numerical noise. The volumes calculated in this way are affected by compression and thermal expansion as well as the reactions since free fluid is always present, but those slowly changing effects give rates only a few percent of the volume change rates during dehydration.

Calculations of cumulative water in pores (Fig. 8a) show a gradual release of water from 0.5 to 1.8 GPa for the hot slab (typified by Kii) but fairly abrupt dehydration at 2.6–3.0 GPa for the cold slab (typified by Hokkaido). Even though total H_2O released is similar for the two p–T paths, the rate of fluid production for cold slabs is an order of magnitude larger (Fig. 8b; note difference in scale for the two curves). It seems likely, given comparable solid viscosities, that the more rapid rate of fluid release would lead to larger stress perturbations upon dehydration.

3.6. Solid volume changes and earthquakes

Solid volume changes during dehydration may inhibit or contribute to earthquake triggering, depending on how they compare with the coincident rate of fluid volume production (Wong et al., 1997; Hacker, 1997). The net change of volume of the full system reaction ΔV_r (solid+fluid) can be positive or negative, which for simple systems leads to increases or decreases in pore fluid pressure respectively. For univariant reactions ΔV_r is inversely proportional to the slope of the reaction boundary by the Clausius–Clapeyron relation. The generation of excess pressure—and hence the tendency toward Coulomb failure—is promoted by reactions where the volume of fluid produced exceeds the reduction in solid volume, $\Delta V_r > 0$; conceptually the creation of fluid outpaces creation of porosity although deformation of the solid will act to balance the two (Wong et al., 1997; Hacker, 1997). In some experiments on antigorite in the presence of shear stress, the introduction of fluids triggered shear failure in antigorite even when $\Delta V_r < 0$ (Jung et al., 2004), but the mechanism by which this occurred is not well understood. More generally, the ability of dehydration to lead to overpressure also depends upon compaction, permeability and fluid flow (Connolly, 1997).

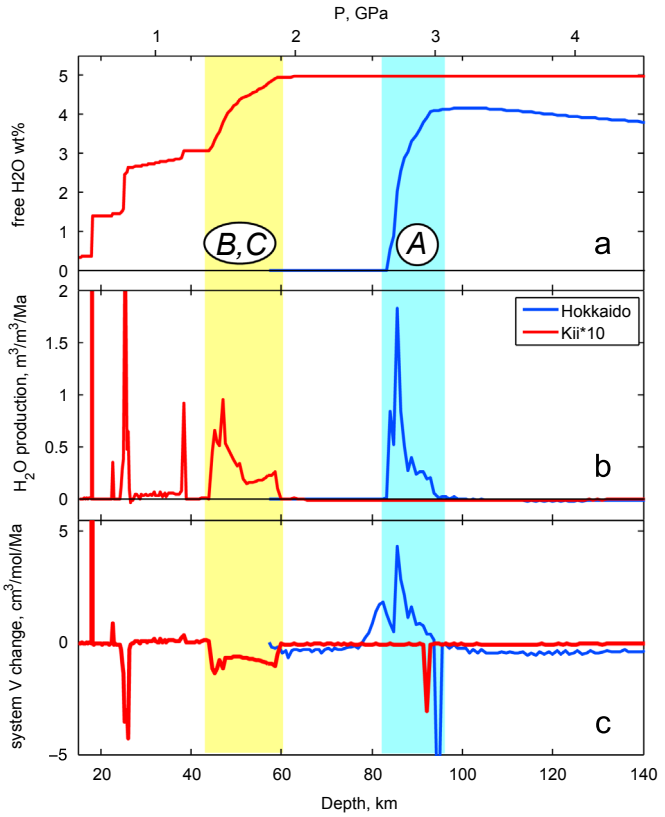

Fig. 8. Evolution of pore fluid pressure and volume calculated for a representative cold slab (Hokkaido; blue) and hot slab (Kii; red). (a) Accumulated dehydration-derived H_2O as wt%. (b) Rate of fluid production in vol%(H_2O)/vol%(total)/Ma, with Kii scaled 10× relative to Hokkaido for clarity. (c) Incremental change in total system (solid+H_2O) volume as dehydration reactions progress, per mol original rock, per Ma. Metamorphic facies including free H_2O are calculated for hydrated MORB along p–T paths from the top of the slab (Fig. 7a). Phase equilibria calculated from Perple_X (Connolly and Petrini, 2002) for a closed system to track total volume in self-consistent manner; estimates assuming total continuous fluid loss are similar. Light blue and yellow regions denote depth intervals of major dehydration for Hokkaido and Kii, respectively, with capital letters denoting specific reactions from Fig. 7. Note the large difference in fluid production rate and the difference in sign of net volume change for these two dehydration events, despite similar total water contents. (For interpretation of the references to color in this figure legend, the reader is referred to the web version of this article.)

Regardless, there appears to be a correlation between reaction volume change and seismic behavior in subduction zones. Where lawsonite breaks down at 3 GPa (640–650 °C) the change in volume of the solids across this reaction, ΔV_S, is −0.10 cm^3/mol and the volume of the reaction, ΔV_r, is +0.032 cm^3/mol. The zoisite breakdown at 2 GPa has a negative Clapeyron slope; the change in volume of the solids across this reaction, ΔV_S, is −0.11 cm^3/mol and the total change in volume of the reaction is also negative, $\Delta V_r = -0.023$ cm^3/mol. Thus, lawsonite breakdown should increase fluid pressure while zoisite breakdown should decrease it.

To illustrate this point for a more complex lithology, we calculate the net system volume change for the MORB–H_2O system for a hot and a cold path (Fig. 8c). For cold slab paths the net system volume increases, or that the volume of fluid generated exceeds the decrease in solid volume in the (lawsonite-breakdown) reactions at 2.6–3.0 GPa. However, in a hot slab the major extended dehydration reactions at 1.4–1.8 GPa show a net negative sign of the system volume change, because the solid is reacting away and densifying faster than H_2O is produced by volume. In other words, the major dehydration reactions in subducted crust lead to conditions favoring increased fluid pressure in cold slabs, but decreased pore pressure in hot slabs. Of course, actual build-up of pressure is highly mediated by permeable flow and deformation-induced changes in porosity, and

will change as earthquakes create fracture conduits and as fluids flow in from deeper reactions. Still, these calculations suggest that the pressure evolution of cold crust favors overpressure while that of hot crust inhibits it, perhaps explaining differences in seismicity between the two types of subduction zones.

4. Summary and conclusions

Earthquakes can occur in the subducted crust, or mantle. In hot subduction zones, earthquakes lie preferentially within subducting mantle, or very close to the subducting Moho. By contrast, in colder subduction zones (everywhere but Nankai, Cascadia, so far examined) earthquakes are abundant within subducting crust, although locally within the subducting mantle as well, in upper-plane seismicity. The crossover between these two classes of subduction zones can be approximated by $\Phi = 500$–1000 km, although it seems likely that details of the p–T path experienced by the subducting crust should be important.

One explanation for this behavior arises from noticing that the p–T trajectories of crust in hot and cold subduction zones cross different reaction boundaries, leading to release of fluids in different ways. Hot subduction zones dehydrate to eclogite via zoisite and amphibole breakdown, which produce H_2O slowly compared with decrease in volume in the solid, driving a net reduction in pore pressure. Cold subduction zones undergo a series of reactions where blueschist breaks down, fairly rapidly and with net system volume increase, a dehydration event that could promote excess pressure. Although the evolution of fluid pressure involves many more factors, the variation in seismicity with reaction behavior confirms that dehydration plays a crucial role in the generation of earthquakes in subduction zones.

Acknowledgments

The ideas presented in this paper nucleated at a Sendai G-COE Symposium (2010) and we thank the conference sponsors. Data in the U.S. were all collected on a variety of projects sponsored by the National Science Foundation (NSF EAR-0545441). Thermal modeling was supported by NSF 0646757 and 084048. This work was supported in part by the Ministry of Education, Culture, Sports, Science and Technology of Japan, under its Observation and Research Program for Prediction of Earthquakes and Volcanic Eruptions, and by the Global COE Program, Global Education and Research Center for Earth and Planetary Dynamics, Tohoku University. LDEO Contribution number 7679.

References

Abers, G.A., van Keken, P.E., Kneller, E.A., Ferris, A., Stachnik, J.C., 2006. The thermal structure of subduction zones constrained by seismic imaging: implications for slab dehydration and wedge flow. Earth Planet. Sci. Lett. 241, 387–397.

Abers, G.A., MacKenzie, L.S., Rondenay, S., Zhang, Z., Wech, A.G., Creager, K.C., 2009. Imaging the source region of Cascadia tremor and intermediate-depth earthquakes. Geology 37, 1119–1122.

Atwater, T., 1989. Plate tectonic history of the northeast Pacific and western North America. In: Winterer, E.L., Hussong, D.M., Decker, R.W. (Eds.), The Eastern Pacific Ocean and Hawaii, The Geology of North America N. Geological Society of America, Boulder, Colorado, pp. 21–72.

Bengtson, A.K., van Keken, P.E., 2012. Three-dimensional thermal structure of subduction zones: effects of obliquity and curvature. Solid Earth Discuss. 4, 919–941.

Bassett, D., Sutherland, R., Henrys, S., Stern, T., Scherwath, M., Benson, A., Toulmin, S., Henderson, M., 2010. Three-dimensional velocity structure of the northern Hikurangi margin, Raukumara, New Zealand: implications for the growth of continental crust by subduction erosion and tectonic underplating. Geochem. Geophys. Geosyst. 11, http://dx.doi.org/10.1029/2010GC003137.

Brown, J.R., Beroza, G., Ide, S., Ohta, K., Shelly, D., Schwartz, S.Y., Rabbel, W., Thorwart, M., Kao, H., 2009. Deep low-frequency earthquakes in the tremor zone localize to the plate interface in multiple subduction zones. Geophys. Res. Lett. 36, L19306, http://dx.doi.org/10.1029/2009GL040027.

Bruns, T.R., 1983. Model for the origin of the Yakutat block, an accreting terrane in the northern Gulf of Alaska. Geology 11, 718–721.

Calkins, J.A., Abers, G.A., Ekström, G., Creager, K.C., Rondenay, S., 2011. Shallow structure of the Cascadia subduction zone beneath western Washington from spectral ambient noise correlation. J. Geophys. Res. 116, http://dx.doi.org/10.1029/2010JB007657. (art. no. B07302).

Christeson, G.L., Gulick, S.P.S., van Avendonk, H.J.A., Worthington, L.L., Reece, R.S., Pavlis, T.L., 2010. The Yakutat terrane: dramatic change in crustal thickness across the Transition fault, Alaska. Geology 38, 895–898.

Clift, P., Vannucchi, P., 2004. Controls on tectonic accretion versus erosion in subduction zones: implications for the origin and recycling of the continental crust. Rev. Geophys. 42, RG2001, http://dx.doi.org/10.1029/2003RG000127.

Connolly, J.A.D., 1997. Devolatilization-generated fluid pressure and deformation-propagated fluid flow during prograde regional metamorphism. J. Geophys. Res. 102, 18,149–18,173.

Connolly, J.A.D., Petrini, K., 2002. An automated strategy for calculation of phase diagram sections and retrieval of rock properties as a function of physical conditions. J. Metamorph. Geol. 20, 697–798.

DeMets, C., Gordon, R.G., Argus, D.F., Stein, S., 1994. Effect of recent revisions to the geomagnetic reversal time-scale to estimates of current plate motions. Geophys. Res. Lett. 21, 2191–2194.

DeShon, H., Schwartz, S., Newman, A., Gonzalez, V., Protti, M., Dorman, L., Dixon, T., Sampson, D., Flueh, E., 2006. Seismogenic zone structure beneath the Nicoya Peninsula, Costa Rica, from three-dimensional local earthquake P- and S-wave tomography. Geophys. J. Int. 164, 109–124.

Dobson, P., Meredith, G., Boon, S.A., 2002. Simulation of subduction zone seismicity by dehydration of serpentine. Science 298, 1407–1410.

Eberhart-Phillips, D., Christensen, D.H., Brocher, T.M., Hansen, R., Ruppert, N.A., Haueussler, P.J., Abers, G.A., 2006. Imaging the transition from Aleutian subduction to Yakutat collision in central Alaska, with local earthquakes and active source data. J. Geophys. Res. 111, B11303, http://dx.doi.org/10.1029/2005JB004240.

Ferris, A., Abers, G.A., Christensen, D.H., Veenstra, E., 2003. High resolution image of the subducted Pacific (?) plate beneath central Alaska, 50–150 km depth. Earth Planet. Sci. Lett. 214, 575–588.

Frohlich, C., 1989. The nature of deep earthquakes. Annu. Rev. Earth Planet. Sci. 17, 227–254.

Fuis, G.S., Moore, T.E., Plafker, G., Brocher, T.M., Fisher, M.A., Mooney, W.D., Nokleberg, W.J., Page, R.A., Beaudoin, B.C., Christensen, N.I., Levander, A.R., Lutter, W.J., Saltus, R.W., Ruppert, N.A., 2008. Trans-Alaska Crustal Transect and continental evolution involving subduction underplating and synchronous foreland thrusting. Geology 36, 267–270.

Green, H.W., Houston, H., 1995. The mechanics of deep earthquakes. Annu. Rev. Earth Planet. Sci. 23, 169–213.

Hacker, B.R., 1997. Diagenesis and the fault-valve seismicity of crustal faults. J. Geophys. Res. 102, 24,459–24,467.

Hacker, B.R., 2008. H_2O subduction beyond arcs. Geochem. Geophys. Geodyn. 9, Q03001, http://dx.doi.org/10.1029/2007GC001707.

Hacker, B.R., Abers, G.A., Peacock, S.M., 2003a. Subduction factory 1: theoretical mineralogy, density, seismic wavespeeds, and H_2O content. J. Geophys. Res. 108, 2029, http://dx.doi.org/10.1029/2001JB001127.

Hacker, B.R., Peacock, S.M., Abers, G.A., Holloway, S.D., 2003b. Subduction Factory 2. Are intermediate-depth earthquakes in subducting slabs linked to metamorphic dehydration reactions? J. Geophys. Res. 108, 2030, http://dx.doi.org/10.1029/2001JB001129.

Hirose, F., Nakajima, J., Hasegawa, A., 2008. Three-dimensional seismic velocity structure and configuration of the Philippine Sea slab in southwestern Japan estimated by double-difference tomography. J. Geophys. Res. 113, http://dx.doi.org/10.1029/2007JB005274.

Ichinose, G.A., Thio, H.K., Somerville, P.G., 2004. Rupture process and near-source shaking of the 1965 Seattle-Tacoma and 2001 Nisqually, intraslab earthquakes. Geophys. Res. Lett. 31, http://dx.doi.org/10.1029/2004GL019668.

Ide, S., Shelly, D.R., Beroza, G.C., 2007. Mechanisms of deep low frequency earthquakes: further evidence that deep non-volcanic tremor is generated by shear slip on the plate interface. Geophys. Res. Lett. 34, http://dx.doi.org/10.1029/2006GL028890.

Igarashi, T., Matsuzawa, T., Umino, N., Hasegawa, A., 2001. Spatial distribution of focal mechanisms for interplate and intraplate earthquakes associated with the subducting Pacific plate beneath the northeastern Japan arc: a tripled-planed deep seismic zone. J. Geophys. Res. 106, 2177–2191.

Ito, Y., Obara, K., Shiomi, K., Sekine, S., Hirose, H., 2007. Slow earthquakes coincident with episodic tremors and slow slip events. Science 315, 503–506.

Jarrard, R.D., 2003. Subduction fluxes of water, carbon dioxide, chlorine and potassium. Geochem. Geophys. Geosyst. 4, 8905, http://dx.doi.org/10.1029/2002GC000392.

Jung, H., Green, H.W., Dobrzhinetskaya, L.W., 2004. Intermediate-depth earthquake faulting by dehydration embrittlement with negative volume change. Nature 428, 545–549.

Kato, A., Iidaka, T., Ikuta, R., Yoshida, Y., Katsumata, K., Iwasaki, T., Sakai, S.i., Thurber, C., Tsumura, N., Yamaoka, K., Watanabe, T., Kunitomo, T., Yamazaki, F., Okubo, M., Suzuki, S., Hirata, N., 2010. Variations of fluid pressure within the subducting oceanic crust and slow earthquakes. Geophys. Res. Lett. 37, L14310.

Kawakatsu, H., Watada, S., 2007. Seismic evidence for deep-water transportation in the mantle. Science 316, 1468–1471.

Kelemen, P.B., Hirth, G., 2007. A periodic shear-heating mechanism for intermediate-depth earthquakes in the mantle. Nature 446, 787–790.
Kim, YH., Abers, G.A., Li, J., Christensen D.H., Calkins, J., 2012. Imaging megathrust and Yakutat/Pacific plate interface in Alaska subduction zone. In: Abstract 1431213, Presented at 2012 Fall Meeting AGU. 3–7 December, San Francisco, California.
Kimura, J.I., Stern, R.J., Yoshida, T., 2005. Reinitiation of subduction and magmatic responses in SW Japan during Neogene time. Geol. Soc. Am. Bull. 117, 969–986.
Kirby, S., Engdahl, E.R., Denlinger, R., 1996. Intermediate-depth intraslab earthquakes and arc volcanism as physical expressions of crustal and uppermost mantle metamorphism in subducting slabs. In: Bebout, G.E., Scholl, D., Kirby, S. (Eds.), Subduction: Top to Bottom, Geophysical Monograph, vol. 96. American Geophysical Union, Washington, DC, pp. 195–214.
Kita, S., Okada, T., Nakajima, J., Matsuzawa, T., Hasegawa, A., 2006. Existence of a seismic belt in the upper plane of the double seismic zone extending in the along-arc direction at depths 70–100 km beneath NE Japan. Geophys. Res. Lett. 33, L24310, http://dx.doi.org/10.1029/2006GL028239.
Kita, S., Okada, T., Hasegawa, A., Nakajima, J., Matsuzawa, T., 2010a. Existence of interplane earthquakes and neutral stress boundary between the upper and lower planes of the double seismic zone beneath Tohoku and Hokkaido, northeastern Japan. Tectonophysics 496, 68–82, http://dx.doi.org/10.1016/j.tecto.2010.10.010.
Kita, S., Okada, T., Hasegawa, A., Nakajima, J., Matsuzawa, T., 2010b. Anomalous deepening of a seismic belt in the upper-plane of the double seismic zone in the Pacific slab beneath the Hokkaido corner: possible evidence for thermal shielding caused by subducted forearc crust materials. Earth Planet. Sci. Lett. 290, 415–426, http://dx.doi.org/10.1016/j.epsl.2009.12.038.
Li, X.Q., Nabelek, J.L., 1999. Deconvolution of teleseismic body waves for enhancing structure beneath a seismometer array. Bull. Seismol. Soc. Am. 89, 190–201.
Lambert, I.B., Wyllie, P.J., 1972. Melting of gabbro (quartz eclogite) with excess water to 35 kilobars, with geological applications. J. Geol. 80, 693–708.
Loveless, J.P., Meade, B.J., 2010. Geodetic imaging of plate motions, slip rates, and partitioning of deformation in Japan. J. Geophys. Res. 115, http://dx.doi.org/10.1029/2008JB006248.
MacKenzie, L.M., Abers, G.A., Rondenay, S., Fischer, K.M., 2010. Imaging a steeply dipping subducting slab in southern Central America. Earth Planet. Sci. Lett. 296, 459–468.
Matsuzawa, T., Umino, N., Hasegawa, A., Takagi, A., 1986. Upper mantle velocity structure estimated from PS-converted wave beneath the north-eastern Japan Arc. Geophys. J. R. Astron. Soc. 86, 767–787.
McKenzie, D.P., 1969. Speculations on the consequences and causes of plate motions. Geophys. J. R. Astron. Soc. 18, 1–32.
Miyazaki, S., Heki, S., 2001. Crustal velocity field of southwest Japan: subduction and arc-arc collision. J. Geophys. Res. 106, 4305–4326.
Molnar, P., Freedman, D., Shih, J.S.F., 1979. Lengths of intermediate and deep seismic zones and temperatures in downgoing slabs of lithosphere. Geophys. J. R. Astron. Soc. 56, 41–54.
Moyen, J.-F., 2011. The composite Archean grey gneisses: petrological significance, and evidence for a non-unique tectonic setting for Archean crustal growth. Lithos 123, 21–36.
Nakajima, J., Tsuji, Y., Hasegawa, A., 2009a. Seismic evidence for thermally-controlled dehydration in subducting oceanic crust. Geophys. Res. Lett. 36, L03303, http://dx.doi.org/10.1029/2008GL036865.
Nakajima, J., Tsuji, Y., Hasegawa, A., Kita, S., Okada, T., Matsuzawa, T., 2009b. Tomographic imaging of hydrated crust and mantle in the subducting, Pacific slab beneath Hokkaido, Japan: evidence for dehydration embrittlement as a cause of intraslab earthquakes. Gondwana Res. 16, 470–481.
Nicholson, T., Bostock, M., Cassidy, J.F., 2005. New constraints on subduction zone structure in northern Cascadia. Geophys. J. Int. 151, 849–859.
Obara, K., 2002. Nonvolcanic deep tremor associated with subduction in southwest Japan. Science 296, 1679–1681.
Ogawa, M., 1987. Shear instability in a viscoelastic material as the cause of deep focus earthquakes. J. Geophys. Res. 92, 13801–13810.
Okino, K., Shimakawa, Y., Nagaoka, S., 1994. Evolution of the Shikoku Basin. J. Geomagn. Geoelectr. 46, 463–479.
Oleskevich, D., Hyndman, R., Wang, K., 1999. The updip and downdip limits to great subduction earthquakes: thermal and structural models of Cascadia, south Alaska, SW Japan, and Chile. J. Geophys. Res. 104, 14965–14991.
Parsons, T., Trehu, A.M., Luetgert, J.H., Miller, K.C., Kilbride, F., Wells, R.E., Fisher, M.A., Flueh, E.R., ten Brink, U.S., Christensen, N.I., 1998. A new view into the Cascadia subduction zone and volcanic arc; implications for earthquake hazards along the Washington margin. Geology 26, 199–202.
Peacock, S.M., Wang, K., 1999. Seismic consequences of warm versus cool subduction metamorphism: examples from southwest and northeast Japan. Science 286, 937–939.
Preston, L.A., Creager, K.C., Crosson, R.S., Brocher, T.M., Trehu, A.M., 2003. Intraslab earthquakes: dehydration of the Cascadia slab. Science 302, 1197–2000.
Raleigh, C.B., Paterson, M.S., 1965. Experimental deformation of serpentinite and its tectonic implications. J. Geophys. Res. 70, 3965–3985.
Rondenay, S., Bostock, M.G., Shragge, J., 2001. Multiparameter two-dimensional inversion of scattered teleseismic body waves, 3, application to the Cascadia 1993 data set. J. Geophys. Res. 106, 30,795–730,808.
Rondenay, S., Abers, G.A., van Keken, P.E., 2008. Seismic imaging of subduction zone metamorphism. Geology 36, 275–278.
Rondenay, S., Montési, L., Abers, G.A., 2010. New geophysical insight into the origin of the Denali volcanic gap. Geophys. J. Int. 182, 613–630.
Rossi, G., Abers, G.A., Rondenay, S., Christensen, D.H., 2006. Unusual mantle Poisson's ratio, subduction, and crustal structure in Central Alaska. J. Geophys. Res. 111, B09311.
Schmidt, M.W., Poli, S., 1998. Experimentally based water budgets for dehydrating slabs and consequences for arc magma generation. Earth Planet. Sci. Lett. 163, 361–379.
Seno, T., Stein, S., Gripp, A.E., 1993. A model for the motion of the Philippine Sea plate consistent with NUVEL-1 and geological data. J. Geophys. Res. 98, 17941–17948.
Shelly, D.R., Beroza, G.C., Nakamula, S., 2006. Low-frequency earthquakes in Shikoku, Japan, and their relationship to episodic tremor and slip. Nature 442, 188–191.
Sodoudi, F., Yuan, X., Asch, G., Kind, R., 2011. High-resolution image of the geometry and thickness of the subducting Nazca lithosphere beneath northern Chile. J. Geophys. Res. 116, http://dx.doi.org/10.1029/2010JB007829.
Stein, C.A., Stein, S., 1992. A model for the global variations in oceanic depth and heat-flow with lithospheric age. Nature 359, 123–129, http://dx.doi.org/10.1038/359123a0.
Syracuse, E.M., Abers, G.A., 2006. Global compilation of variations in slab depth beneath arc volcanoes and implications. Geochem. Geophys. Geodyn. (G3) 7, Q05017, http://dx.doi.org/10.1029/2005GC001045.
Syracuse, E.M., van Keken, P.E., Abers, G.A., 2010. The global range of subduction zone thermal models. Phys. Earth Planet. Inter. 183, 73–90, http://dx.doi.org/10.1016/j.pepi.2010.1002.1004.
Tanaka, A., Yamano, M., Yano Y., Sasada, M., 2004, Geothermal Gradient and Heat Flow Data In and Around Japan. Digital Geoscience Map DGM P-5, Geological Survey of Japan.
Takahashi, N., Kodaira, S., Tsuru, T., Park, J.-O., Kaneda, Y., Suyehiro, K., Kinoshita, H., Abe, S., Nishino, M., Hino, R., 2004. Seismic structure and seismogenesis off Sanriku region, northeastern Japan. Geophys. J. Int. 159, 129–145.
Tsuji, Y., Nakajima, J., Hasegawa, A., 2008. Tomographic evidence for hydrated oceanic crust of the Pacific slab beneath northeastern Japan: implications for water transportation in subduction zones. Geophys. Res. Lett. 35, L14308, http://dx.doi.org/10.1029/2008GL034461.
Uchida, N., Nakajima, J., Hasegawa, A., Matsuzawa, T., 2009. What controls interplate coupling?: evidence for abrupt change in coupling across a border between two overlying plates in the NE Japan subduction zone. Earth Planet. Sci. Lett. 283, 111–121.
van Keken, P.E., Hacker, B.R., Syracuse, E.M., Abers, G.A., 2011. Subduction Factory 4: depth-dependent flux of H_2O from subducting slabs worldwide. J. Geophys. Res. 116, http://dx.doi.org/10.1029/2010JB007922. (art. no. B01401).
van Keken, P.E., Kita, S., Nakajima, J., 2012. Thermal structure and intermediate-depth seismicity in the Tohoku-Hokkaido subduction zones. Solid Earth Discuss. 4, 1069–1093.
Vielzeuf, D., Schmidt, D.W., 2001. Melting relations in hydrous systems revisited: applications to metapelites, metagreywackes and matabasalts. Contrib. Mineral. Petrol. 141, 251–267.
Wada, I., Wang, K., 2009. Common depth of slab-mantle decoupling: reconciling diversity and uniformity of subduction zones. Geochem. Geophys. Geosyst. 10, Q10009.
Wada, I., Mazzotti, S., Wang, K., 2010. Intraslab stresses in the Cascadia subduction zone from inversion of earthquake focal mechanisms. Bull. Seismol. Soc. Am. 100, 2002–2013.
Wadati, K., 1928. Shallow and deep earthquakes. Geophys. Mag. 1, 161–202.
Wong, T.-F., Ko, S.C., Olgaard, D.L., 1997. Generation and maintenance of pore pressure excess in a dehydrating system, 2, theoretical analysis. J. Geophys. Res. 102, 841–852.
Worthington, L.L., van Avendonk, H.J.A., Gulick, S.P.S., Christeson, G.L., Pavlis, T.L., 2012. Crustal structure of the Yakutat terrane and the evolution of subduction and collision in southern Alaska. J. Geophys. Res. 117, http://dx.doi.org/10.1029/2010TC002723.
Yamauchi, M., Hirahara, K., Shibutani, T., 2003. High resolution receiver function imaging of the seismic velocity discontinuities in the crust and the uppermost mantle beneath southwest Japan. Earth Planets Space 55, 59–64.
Yuan, X., Sobolev, S.V., Kind, R., Oncken, O., Bock, G., Asch, G., Schurr, B., Graeber, F., Rudloff, A., Hanka, W., Wylegalla, K., Tibi, R., Haberland, C., Rietbrock, A., Giese, P., Wigger, P., Rower, P., Zandt, G., Beck, S., Wallace, T., Pardo, M., Comte, D., 2000. Subduction and collision processes in the Central Andes constrained by converted seismic phases. Nature 408, 958–961.
Zhao, D., Matsuzawa, T., Hasegawa, A., 1997. Morphology of the subducting slab boundary in the northeastern Japan arc. Phys. Earth Planet. Inter. 102, 89–104.